PHOTONICS Research

Plasmonic resonant nonlinearity and synthetic optical properties in gold nanorod suspensions

Huizhong Xu,[1] Pepito Alvaro,[1] Yinxiao Xiang,[1] Trevor S. Kelly,[1] Yu-Xuan Ren,[1] Chensong Zhang,[1] and Zhigang Chen[1,2,*]

[1]Department of Physics and Astronomy, San Francisco State University, San Francisco, California 94132, USA
[2]TEDA Applied Physics Institute and School of Physics, Nankai University, Tianjin 300457, China
*Corresponding author: zhigang@sfsu.edu

Received 28 August 2018; revised 26 October 2018; accepted 31 October 2018; posted 2 November 2018 (Doc. ID 344401); published 11 December 2018

We experimentally demonstrate self-trapping of light, as a result of plasmonic resonant optical nonlinearity, in both aqueous and organic (toluene) suspensions of gold nanorods. The threshold power for soliton formation is greatly reduced in toluene as opposed to aqueous suspensions. It is well known that the optical gradient forces are optimized at off-resonance wavelengths at which suspended particles typically exhibit a strong positive (or negative) polarizability. However, surprisingly, as we tune the wavelength of the optical beam from a continuous-wave (CW) laser, we find that the threshold power is reduced by more than threefold at the plasmonic resonance frequency. By analyzing the optical forces and torque acting on the nanorods, we show theoretically that it is possible to align the nanorods inside a soliton waveguide channel into orthogonal orientations by using merely two different laser wavelengths. We perform a series of experiments to examine the transmission of the soliton-forming beam itself, as well as the polarization transmission spectrum of a low-power probe beam guided along the soliton channel. It is found that the expected synthetic anisotropic properties are too subtle to be clearly observed, in large part due to Brownian motion of the solvent molecules and a limited ordering region where the optical field from the self-trapped beam is strong enough to overcome thermodynamic fluctuations. The ability to achieve tunable nonlinearity and nanorod orientations in colloidal nanosuspensions with low-power CW laser beams may lead to interesting applications in all-optical switching and transparent display technologies.

https://doi.org/10.1364/PRJ.7.000028

1. INTRODUCTION

The study of optical nonlinearities in plasmonic nanostructures and nanocomposites has attracted much attention in recent years [1–5]. As a result of strongly enhanced fields with subwavelength confinement and high sensitivity to the environment, plasmonic nanostructures exhibit unique nonlinear optical phenomena with potential applications in all-optical switching and modulation [6] and sensing [7]. Among the plasmonic nanocomposite systems studied, colloidal suspensions of plasmonic nanoparticles are particularly interesting due to the possibility of manipulating these systems by mechanical, electrical, and optical methods. Previously, third-order optical nonlinearities in colloidal suspensions of gold nanoparticles of different shapes have been studied [8,9]. Self-focusing of a 532 nm laser beam and optical soliton has been demonstrated in plasmonic nanosuspensions of gold nanoparticles and core–shell particles [10]. Furthermore, the propagating self-trapped laser beam forms a soliton channel, a self-induced waveguide, and the guidance of a low-intensity probe beam inside such a channel has also been observed [11,12].

In addition to optical nonlinearity, it may be possible to align gold nanorods using optical fields as suggested theoretically [13,14]. The collective alignment of a large quantity of gold nanorods in a liquid environment may lead to macroscopic anisotropic optical response and can find applications in information processing and display technologies. While ordering of an ensemble of rods has been demonstrated with techniques including applying electric fields [15–20], self-assembly based fabrication [21–23], the stretched-film method [24–26], and the electrospinning technique [27,28], so far only manipulation of individual plasmonic nanorods was demonstrated experimentally with optical traps [29–34]. Recently, we attempted to achieve orientational ordering of gold nanorods inside an optical soliton channel established by pumping a colloidal suspension of gold nanorods with a 532 nm laser beam [35]. In the study, transmission as a function of the polarization direction

of a linearly polarized low-intensity 1064 nm probe beam was measured, providing indirect evidence for the presence of nanorod ordering in the system. However, the input power of the probe beam was not fixed for different polarizations, which may complicate the interpretation of the experimental results. Furthermore, control of nanorod alignment via plasmonic resonant tuning remains elusive.

In this work, we study optical nonlinearity in suspensions of gold nanorods and explore the effect of the solvent environment (aqueous versus organic) on soliton formation. Toluene is chosen as the organic solvent here, motivated by previous reports of obtaining good alignment of gold nanorods in toluene by applying an electrical field [18,19]. The threshold power for soliton formation for both suspensions is measured as a function of wavelength. We then analyze the optical forces exerted on the nanorods and discuss their role in the formation of solitons. By analyzing the optical torque acting on the nanorods and associated rotational potential energy, we show theoretically that it is possible to align the nanorods inside a soliton channel, leading to wavelength-dependent orientations. Finally, we perform polarization transmission measurements of a low-power probe beam (at 1064 nm) guided along the soliton channel to obtain information about soliton-mediated anisotropic optical properties of the colloidal suspensions.

2. EXPERIMENTAL SETUP

In a typical experiment, a cuvette with 5 mL of the nanorod solution (Nanopartz, Part #A12-50-800 for aqueous suspension and #E12-50-800-NPO-TOL for toluene suspension) is used in the optical path, as shown in Fig. 1. A continuous-wave (CW) laser beam of tunable wavelength is focused into the sample, driving the nanorods to form a soliton channel, and will be referred as the pump (soliton-forming) beam in this study. The input power of the pump beam can be varied from 0 to 1000 mW by a half-wave plate mounted on a step motor. The profile of the soliton beam is recorded with a CCD camera at the input and at the output when the beam exits from the sample. The power transmission of the soliton beam is measured for a range of wavelengths by recording both the input and output power. To measure the optical anisotropy of the soliton channel, a 1064 nm probe beam from a CW laser with a fixed power for different polarizations, which can be tuned by a polarizer placed before the dichroic mirror, is then guided through the soliton channel. Since the probe beam has a very low power and is at a wavelength that does not favor the nonlinear self-action of the beam, it will not interfere with the formation of a soliton by the pump beam. The power of the output probe beam after the sample is then measured with the use of a long-pass filter to remove the pump beam and a pinhole to exclude the probe beam that is outside the soliton channel. The formation of the soliton beam and the guidance of the probe beam along the soliton channel are also verified by recording their side-view images, as shown in the inset of Fig. 1.

3. RESULTS AND DISCUSSION

A. Solvent-Dependent Nonlinear Response

By sending a focused, linearly polarized 740 nm pump beam at varying input powers into a 1.25-cm-long cuvette of gold nanorods (average diameter 50 nm, average length 145 nm) suspended in water or toluene, we compare the nonlinear effects of gold nanorods in two different suspensions. The optical densities of the samples are matched by diluting the toluene solution (Part #E12-50-800-NPO-TOL) obtained from Nanopartz to the same as the aqueous solution (Part #A12-50-800). For both cases, when an input beam at 10 mW is applied [see Figs. 2(a) and 2(e)], an output beam exhibiting linear diffraction is observed [see Figs. 2(b) and 2(f)]. For the aqueous plasmonic solution, linear diffraction of the beam dominates for input pump power up to 50 mW. At an input pump power of 157 mW, nonlinear focusing starts to have an effect and the output beam size starts to decrease [see Fig. 2(c)] compared to the beam sizes at lower pump powers. The output beam size is further reduced with increasing pump power, and nonlinear self-trapping is observed at a pump power of 620 mW [see Fig. 2(d)], indicating the formation of a soliton beam. In the case of the toluene solution, nonlinear focusing starts to have an effect on the output beam profile for a pump power as low as 50 mW [see Fig. 2(g)]. However, at an input power of 157 mW,

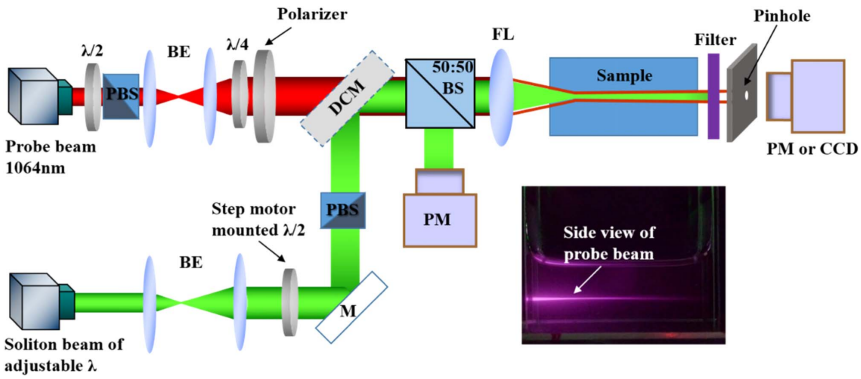

Fig. 1. Schematic of the experimental setup. A linearly polarized 1064 nm probe beam is sent through a soliton channel created by a pump beam of tunable wavelength from 700 to 960 nm in a suspension of gold nanorods. The polarizer before the dichroic mirror is to establish a linearly polarized light for the probe beam. BE, beam expander; DCM, dichroic mirror; FL, focusing lens; M, mirror; PBS, polarizing beam splitter; PM, powermeter. The insert shows the guidance of an infrared probe beam of 1064 nm wavelength through a 4-cm-long cuvette of gold nanoparticle suspension by a soliton-induced waveguide formed typically at a visible wavelength of 532 nm.

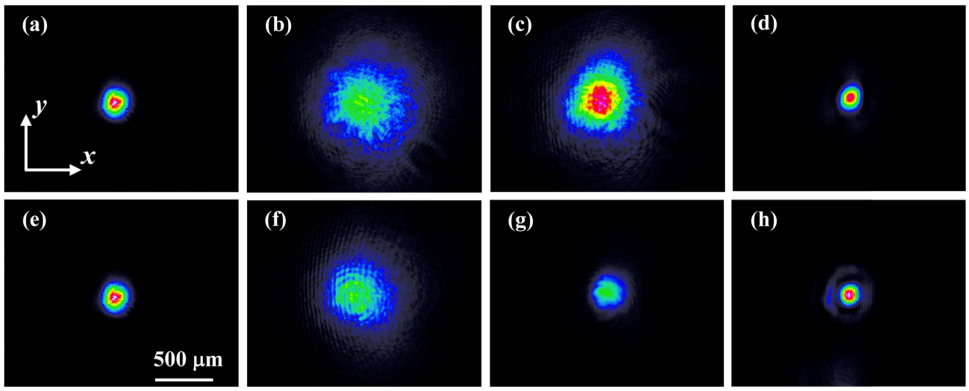

Fig. 2. Beam profiles of a 740 nm laser soliton beam passing through a suspension of gold nanorods (average diameter 50 nm, average length 145 nm) in water (top panels) and toluene (bottom panels) at different powers. (a) Input beam profile at 10 mW. (b)–(d) Output beam profiles pumped at 10, 157, and 620 mW, respectively. (e) Input beam profile at 10 mW. (f)–(h) Output beam profiles pumped at 10, 50, and 157 mW, respectively. Note the significant decrease in threshold power for self-trapping in toluene solution.

nonlinear self-trapping of the input beam to form a soliton is observed [see Fig. 2(h)], indicating a significant decrease in threshold power. We note that the ring structures in Fig. 2(h) are a result of thermal defocusing, which has been reported previously [36].

As seen from Fig. 2, the necessary input power needed to create a soliton is significantly different for the aqueous and toluene samples. Given that the dimensions of the gold rods and the input beam sizes [see Figs. 2(a) and 2(e)] are the same for the two types of samples, a possible explanation for the different level of optical nonlinearity observed here could be that water and toluene have different values of refractive index and viscosity, which can affect the motion of nanorods in the solvent. We have found that the values of nanorod polarizability and extinction cross section are similar for the aqueous and toluene suspensions due to the small difference in their refractive indices. On the other hand, viscosity affects the translational motion of the rods. Since the two solvents have very different values of viscosity, we believe the viscosity of the background medium plays a major role in determining the soliton threshold power and have provided a detailed analysis of the optical forces and their effect on optical nonlinearity in Section 3.C. Furthermore, while the exact mechanism is not yet clear, we believe viscosity also affects the rotational dynamics of the rods and the degree of nanorod alignment at equilibrium. More specifically, the viscosity of toluene reported in the literature is smaller than that of water, enabling the orientations of gold nanorods to be readily controlled by an external field [18,19].

B. Wavelength-Dependent Nonlinear Response

The creation of soliton beams in both water and toluene is verified over a wide range of wavelengths from 700 to 960 nm by examining the output profile of the soliton-forming pump beam. At each wavelength, similar to what is observed in Fig. 2, the output beam size decreases as the power of the pump beam increases, and the power corresponding to the smallest output beam size is recorded and is shown in Fig. 3(a) for a toluene suspension of gold nanorods. We find the soliton power varies between 40 and 185 mW for wavelengths ranging from 800 to 950 nm and reaches a minimum of 40 mW at 880 nm, indicating the strongest optical nonlinearity at this wavelength. We note a similar resonant behavior is observed for the aqueous suspension, except that the soliton powers are much higher (~500 mW) and the minimum power occurs around 790 nm.

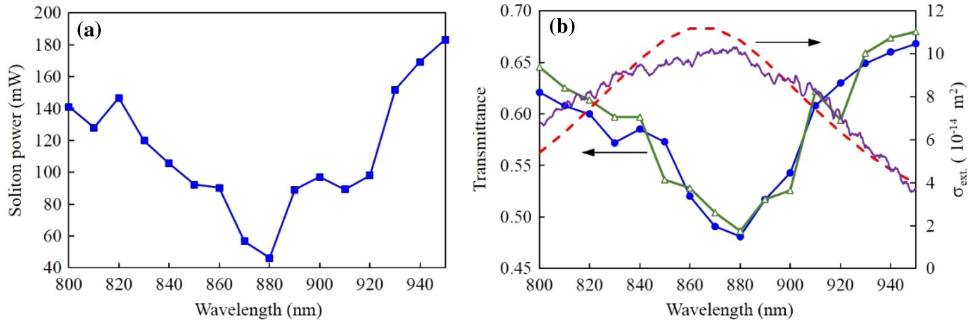

Fig. 3. Threshold power for self-trapping and transmission spectrum of the pump beam through a gold nanorod (average diameter 50 nm, average length 145 nm) suspension in toluene. (a) Soliton-formation power as a function of pump wavelength. (b) Transmission spectra (left axis) of the pump beam for two different input powers: 1 mW (solid circles) for linear propagation and threshold power for soliton formation (open triangles) as shown in (a), and calculated parallel extinction cross sections (dashed line, right axis) of a single nanorod as a function of wavelength and measured white-light extinction spectrum (solid line, arbitrary units, right axis).

The properties of the pump beam in the toluene solution are further explored by measuring the transmission spectra of the soliton beam at different input powers. The results are shown in Fig. 3(b). We find the transmission spectra are independent of the input power of the pump beam, and display a clear transmission minimum (extinction peak) at 880 nm, in good agreement with the predicted longitudinal surface plasmon resonance (LSPR) of gold nanorods in toluene [dashed line in Fig. 3(b)] and the measured white-light extinction spectrum [solid line in Fig. 3(b)]. Remarkably, the wavelength of maximum nonlinearity in Fig. 3(a) corresponds well to the minima in the transmission spectra in Fig. 3(b). In other words, the system exhibits strongest optical nonlinearity at the extinction peak.

C. Optical Forces and Plasmonic Resonant Nonlinearity

To understand the solvent- and wavelength-dependent behavior of solitons in suspensions of gold nanorods, we need to analyze the optical forces exerted on the rods. To do that, we have numerically calculated the polarizabilities for gold nanorods in toluene. The results are shown in Fig. 4(a). We find the real part of the polarizability along the short axis of a nanorod, $\alpha_{\perp}$, stays positive throughout the wavelength range [dashed line in Fig. 4(a)], but for the polarizability along the long axis, $\alpha_{//}$, its real part has a longitudinal surface plasmon resonance around 865 nm, so it can be positive or negative depending on the wavelength [solid line in Fig. 4(a)]. We have also performed similar calculations for gold nanorods in an aqueous suspension. The results are quite similar to those obtained for toluene suspensions, with the major difference being the shift of the LSPR to 790 nm.

Because of the wavelength-dependent polarizabilities, the optical forces acting on the nanorods in the suspension are different when pumped by a linearly polarized laser beam of different wavelengths. For particle size smaller than the incident wavelength (Rayleigh regime), the gradient force is related to the particle's polarizability by [37–40]

$$\vec{F}_{\text{grad}} = \frac{\text{Re}(\alpha)}{4}\nabla|\vec{E}|^2. \tag{1}$$

Therefore, nanorods are attracted to or repelled from the center of the beam depending on the sign of the polarizability. Specifically, if a laser beam has a wavelength below the LSPR of 865 nm, nanorods oriented perpendicular (parallel) to the beam polarization will be attracted to (repelled from) the center of the beam due to the positive (negative) real part of the polarizability $\alpha_{\perp}(\alpha_{//})$. Such optical-force-induced particle motion produces a redistribution of the particle concentration, resulting in an intensity-dependent contrast in refractive index and the subsequent creation of soliton channels in nanosuspensions [10,11,37]. On the other hand, for pump wavelengths above 865 nm, where the real parts of both $\alpha_{\perp}$ and $\alpha_{//}$ are positive, nanorods of both orientations will be attracted to the center of the beam. In both wavelength regimes, a higher refractive index can be effectively induced in the center of the beam under proper conditions, although all positive polarizabilities tend to develop unstable soliton propagation when the intensity-dependent nonlinearity is too high [37–39].

In addition to the gradient force, gold nanorods will also experience the absorption and scattering forces that point in the direction of the Poynting vector [41,42]:

$$\vec{F}_{\text{scat}} = \frac{n_b\sigma_{\text{scat}}}{c}\langle\vec{S}\rangle, \tag{2a}$$

$$\vec{F}_{\text{abs}} = \frac{n_b\sigma_{\text{abs}}}{c}\langle\vec{S}\rangle, \tag{2b}$$

where n_b is the refractive index of the background medium (the solvent), σ_{scat} and σ_{abs} are the scattering and absorption cross sections, respectively, and $\langle\vec{S}\rangle$ is the time-averaged Poynting vector. The sum of these forces is proportional to the extinction cross section σ_{ext}, which is dependent on the orientation of the nanorods. As shown in Fig. 4(b), the perpendicular extinction section is approximately 2 orders of magnitude smaller than the parallel one and displays a monotonic behavior for the wavelength region considered here. Thus, scattering and absorption experienced by the nanorods orientated parallel to the polarization of the pump beam are primarily responsible for the observed minimum in the transmission spectra of the pump beam shown in Fig. 3(b).

If the gradient force plays the main role in the observed optical nonlinearity in suspensions of gold nanorods, we would expect smaller soliton powers at 800 and 940 nm, where the magnitude of the parallel polarizability reaches local maxima.

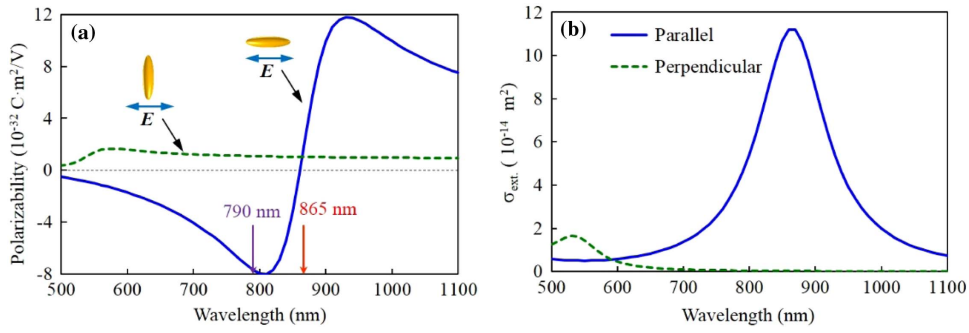

Fig. 4. (a) Real part of the polarizabilities calculated for a single nanorod (diameter 50 nm, length 145 nm) suspended in toluene as a function of wavelength. The perpendicular component (dashed line) stays positive, while the parallel one (solid line) changes from negative to positive as the wavelength is tuned through the LSPR at 865 nm. The two vertical arrows mark the locations of LSPR for rods in water (790 nm) and toluene (865 nm). (b) Calculated parallel (solid line) and perpendicular (dotted line) extinction cross sections of a single nanorod as a function of wavelength.

Instead, we find the smallest soliton power occurs at a wavelength of around 880 nm [Fig. 3(a)], where the extinction cross section reaches a maximum. This suggests that the scattering and absorption forces may play an important role in the formation of solitons for the suspensions of gold nanorods studied here. As a result of the scattering and absorption forces, we expect the rods would be pushed forward with a longitudinal velocity proportional to the sum of the two forces and inversely proportional to the viscosity of the solvent medium:

$$\vec{v} \propto \frac{\vec{F}_{\text{scat}} + \vec{F}_{\text{abs}}}{\eta} \propto \frac{n_b \sigma_{\text{ext}}}{\eta} \langle \vec{S} \rangle. \tag{3}$$

For the range of wavelengths studied here, the longitudinal velocity for parallel rods will be much larger than that for perpendicular rods due to the difference in their extinction cross sections [Fig. 4(b)]. Thus, it is the longitudinal motion of the parallel rods that is responsible for the observed reduction in soliton power near the LSPR. By having the rods move at certain speeds, the concentration of parallel rods inside the soliton channel can be kept at a certain level, thus preventing excessive attenuation of the pump beam along the propagation direction. Compared with off-resonance wavelengths, the extinction cross section near the LSPR is largest, and therefore less power is needed to have the same longitudinal velocity. This is consistent with our observation that the smallest pump power is needed for soliton formation near the extinction peak. We note that it is possible that the velocity of the rods for wavelengths near the LSPR may have to be larger than for off-resonance wavelengths. As the rods move faster, they will spend less time moving across the channel, leading to a decrease in the concentration of parallel rods inside the channel. This will prevent significant attenuation of the pump beam along the propagation direction at the LSPR where the extinction cross section is greatest.

According to Eq. (3), the solvent can affect the velocity of the nanorods through the refractive index of the background medium, the extinction cross section, and the viscosity. The values of extinction cross sections near their respective LSPRs are similar for water and toluene, the refractive index of toluene (1.48) is slightly larger than that of water (1.33), and the viscosity of toluene (0.554 mPa · s at 25°C and 0.1 MPa) [43] is smaller than that of water (0.890 mPa · s at 25°C and 0.1 MPa) [44]. Thus, a smaller pump power is needed in toluene suspensions than in water to generate the same longitudinal velocity, consistent with our observations.

D. Optical Torque and Nanorod Orientation

Next, we consider nanorod orientation inside the soliton-induced waveguide channel. Using finite element method simulations, we calculated the optical torque acting on individual nanorods and found that the nanorods inside the soliton channel tend to align themselves with respect to the polarization of the soliton beam. The rotational potential energy of a nanorod, PE(β), for an arbitrary orientation angle β between the long axis of the rod and the polarization of the pump beam (the x axis), is defined as

$$\text{PE}(\beta) = -\int_0^{\beta} \tau(\theta) \mathrm{d}\theta, \tag{4}$$

where $\tau(\theta)$ is the component of the torque exerted on a nanorod placed at the focus of the pump beam along the beam propagation direction (the z axis). By calculating the torque, we have obtained PE(β) as plotted in Fig. 5.

As shown in Fig. 5(a), the rotational potential energy is minimum at 90° for nanorods located at the focus of a 740 nm laser beam (solid line) with a power of 100 mW and a Gaussian beam radius of 10 μm. The depth of the potential well is about 3 times larger than $k_B T/2 \sim 2.1 \times 10^{-21}$ J, the thermal energy responsible for Brownian motion and disordering of nanorods. Therefore, for this pump wavelength, the torque has a tendency to keep the rods aligned perpendicular to the beam polarization, as schematically shown in Fig. 5(b). However, for a 960 nm laser beam, the minimum of the rotational potential energy occurs at 0° (dashed line), and thus the rods tend to align themselves parallel to the polarization of the pump beam [Fig. 5(b)]. As a result of the wavelength-dependent polarizability, the torque is also wavelength dependent. We find the rods tend to orient themselves parallel (perpendicular) to the direction of the pump polarization for wavelengths above (below) the LSPR, which is

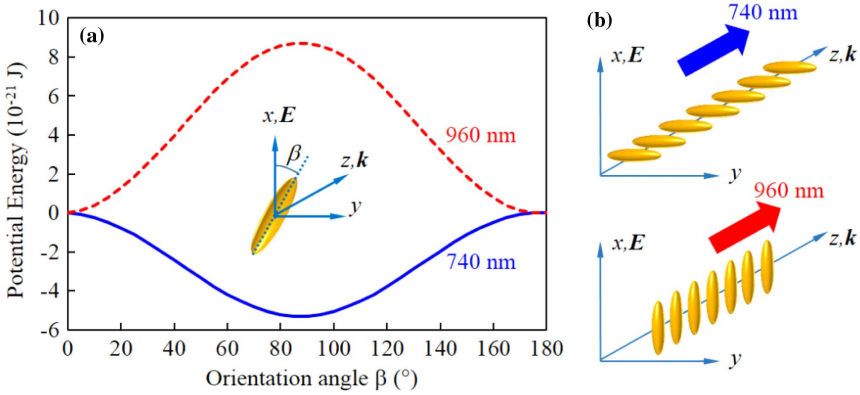

Fig. 5. (a) Calculated potential energy for rotation along the z axis (the beam propagation direction) as a result of the soliton beam acting on a single gold nanorod in toluene at the beam center for two soliton wavelengths: 740 nm (solid line) and 960 nm (dotted line). The soliton beam is assumed to have a power of 100 mW and a Gaussian beam radius of 10 μm. The inset shows the definition of the orientation angle β. Note that the rotational potential energies in the x and y directions (not shown here) are typically 3 orders of magnitude smaller. (b) Schematic illustration of perpendicular and parallel orientations of the nanorods for two soliton wavelengths of 740 and 960 nm, respectively.

consistent with the preferred orientations obtained from analyzing the optical forces as discussed in Section 3.C.

E. Soliton-Mediated Anisotropic Optical Property

Because of the intrinsic anisotropic property of the nanorods, the different orientations of nanorods inside the soliton channel should result in synthetic anisotropic optical properties at the macroscopic scale. The anisotropic properties of the synthetic material created by the soliton beam can be characterized by measuring the polarization transmission spectrum of a probe beam linearly polarized at an angle of θ_1 with respect to the polarization of the soliton beam (the x axis) through the soliton channel. As a result of the difference between the refractive indices along the two principal axes (x and y) of the synthetic material, the output beam generally turns elliptically polarized after passing through the sample. This can be characterized by measuring the intensity transmitted through a polarizer placed after the sample as a function of the polarizer's angle θ_2 with respect to the x axis, given by

$$\begin{aligned} I &= \langle |E(\theta_2)|^2 \rangle \\ &= I_0 \Big(e^{-\eta} \cos^2\theta_1 \cos^2\theta_2 + e^{\eta} \sin^2\theta_1 \sin^2\theta_2 \\ &\quad + \frac{1}{2} \sin 2\theta_1 \sin 2\theta_2 \cos\delta \Big), \end{aligned} \tag{5}$$

where $I_0 = \frac{1}{2}|E_{\text{in}}|^2 \exp\{-[\text{Im}(n_x) + \text{Im}(n_y)]k_0 L\}$, with E_{in} being the input electric field amplitude, n_x and n_y the two refractive indices along two principal axes, respectively, $k_0 L = 2\pi L/\lambda$ the optical phase that the beam accumulates when passing through the suspension of length L, and $\delta = [\text{Re}(n_x) - \text{Re}(n_y)]k_0 L$ and $\eta = [\text{Im}(n_x) - \text{Im}(n_y)]k_0 L$ describe the induced birefringent and dichroic properties of the synthetic material, respectively. If the orientation of the rods is dependent on the wavelength of the pump beam, we expect both the sign and value of $\text{Im}(n_x) - \text{Im}(n_y)$ should change and the major axis of the output probe beam should rotate differently. The total output intensity of the probe beam for a given polarization θ_1 of the input probe beam can be obtained as

$$\begin{aligned} \langle |E|^2 \rangle = \frac{1}{2}|E_{\text{in}}|^2 \Big\{ &\exp\Big[-2\,\text{Im}(n_x)k_0 L\Big]\cos^2\theta_1 \\ &+ \exp\Big[-2\,\text{Im}(n_y)k_0 L\Big]\sin^2\theta_1 \Big\}. \end{aligned} \tag{6}$$

Thus, by measuring the total transmission T of the probe beam at $\theta_1 = 0°$ and 90°, we will be able to obtain the synthetic dichroic property η:

$$\eta = [\text{Im}(n_x) - \text{Im}(n_y)]k_0 L = \ln\sqrt{T(90°)/T(0°)}. \tag{7}$$

Assuming perfect ordering of the gold nanorods inside the soliton channel, we can estimate the corresponding effective refractive indices from the parallel and perpendicular polarizabilities of the rods [Fig. 4(a)] and the Clausius–Mossotti relation:

$$\frac{n_{\text{eff}}^2 - n_b^2}{n_{\text{eff}}^2 + 2n_b^2} = \frac{N\alpha}{3\varepsilon_0 n_b^2}, \tag{8}$$

where n_{eff} and n_b are the effective refractive index of the suspension and the refractive index of the solvent, respectively, N is the number density of nanorods, and α is the nanorod polarizability. Using the number density of 7.36×10^{15} m^{-3} for the toluene suspension, and toluene's refractive index of 1.4812 at 1064 nm, we estimate the real and imaginary part differences between the parallel and perpendicular effective refractive indices of the suspension at the probe wavelength of 1064 nm to be 3.4×10^{-5} and 1.0×10^{-5}, respectively.

To examine the ordering effects in nanorod suspensions as discussed above, we perform a series of polarization transmission measurements with a linearly polarized 1064 nm probe beam guided through the soliton channel (see Fig. 1 for the experimental setup). The input power of the probe beam is fixed at 5.0 mW, and the probe beam itself does not experience appreciable nonlinear self-action, so it will not interfere with the alignment of the rods in the suspensions since the soliton beam has a much higher input power. As a typical example, the measured transmission of the probe beam for a 740 nm pump beam at various powers is shown in Fig. 6. We see a threefold increase in transmission of the probe beam when the power of the pump beam is increased to achieve nonlinear self-trapping, indicating guidance of the probe beam by the soliton channel induced by the pump beam. However, a decrease in transmission for pump powers exceeding 150 mW is observed, since thermal defocusing starts to affect the formation of solitons and thus the guidance.

Transmission spectra of a probe beam with polarizations perpendicular [crosses in Fig. 6(a)] and parallel [open circles

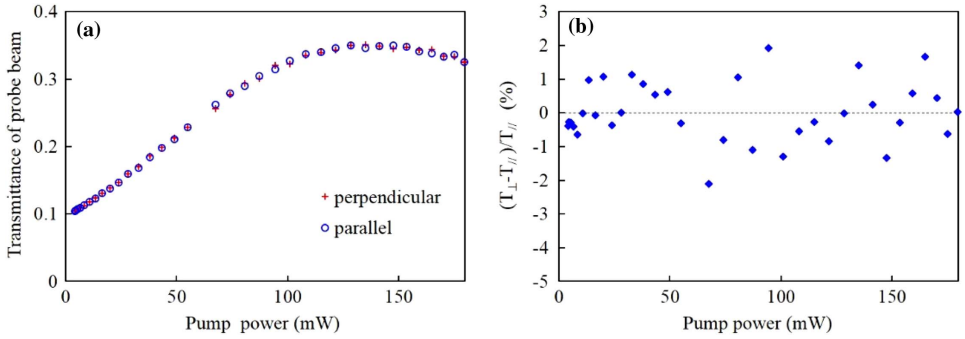

Fig. 6. (a) Transmittance of a 1064 nm probe beam guided by a 740 nm soliton beam as a function of the pump power for probe polarization perpendicular (crosses) and parallel (open circles) to the polarization of the soliton beam. The input power of the probe beam is fixed at 5.0 mW. (b) Relative percentage difference between the perpendicular and parallel transmittances.

in Fig. 6(a)] to the pump beam polarization are measured. No appreciable difference between the two transmittances is observed. The percentage difference between the two [see Fig. 6(b)] is within 2%, a result consistently observed during several repeated measurements. With a theoretically estimated value of 1.0×10^{-5} for $\mathrm{Im}(n_x) - \mathrm{Im}(n_y)$ obtained assuming the rods were fully ordered and $k_0 L$ to be 7.4×10^4 for our sample, we would expect the perpendicular transmittance to be 4.4 times greater than that for the parallel transmittance. The discrepancy between the theoretical expectation and the experimental observation can be attributed to two possible reasons: first, the rods are not fully aligned due to thermodynamic fluctuations caused by Brownian motion of the solvent molecules, and second, ordering probably occurs over a local region near the focus of the laser beam where the optical field is strong and does not extend along the entire beam path as a result of the expansion and attenuation of the pump beam. The pump beam intensity at the focus is strong enough for oriented rods to overcome thermal fluctuations; however, the intensity drops quickly along the lateral direction. The depth of the potential well becomes comparable to the thermal energy at a radius of 7.5 μm and is only 40% of the thermal energy at a radius equal to the beam radius of 10 μm. Therefore, it is unlikely that rods are fully ordered over the entire cross section of the pump beam. This can possibly reduce $\mathrm{Im}(n_x) - \mathrm{Im}(n_y)$ to a fraction of its value in the fully ordered case. As the pump beam propagates along the soliton channel, it also attenuates and expands. We estimate the beam size at output to be approximately 3 times its size at the focus. As a result, the laser beam intensity outside the focus region will not be strong enough to overcome thermal fluctuations to align the nanorods. This will cause the action length to be significantly smaller than the sample length, thus effectively reducing $k_0 L$. Both scenarios will cause the transmission of the probe beam to be insensitive to its polarization. Assuming that $\mathrm{Im}(n_x) - \mathrm{Im}(n_y)$ becomes 3 times smaller than in the fully ordered case, and ordering only occurs over an action length of 500 μm (50 times the beam radius at the focus), we find the percentage difference between the perpendicular and parallel transmittances will be within 2%, a result consistently observed in our experiments. We want to point out that the conclusion drawn here does not match with that from our previous report [35], where an aqueous suspension of gold nanorods was pumped by a 532 nm laser beam and the polarization-dependent transmission of a probe beam appeared to be identified. After a careful examination of the previous results and a series of new experiments performed in the same setting, we found that the apparent polarization-dependent transmission was observed in experiments where the power of the probe beam input to the sample was not fixed when its polarization was adjusted with polarization optics. The underlying mechanism for this phenomenon is not quite clear, though, and we believe it may be related to interactions between the soliton beam and the probe beam. In any case, it is with no doubt that nanorods can be aligned by high electric fields [18–20], so the proposed scheme in Fig. 5(b) and associated anisotropic optical properties should be achievable with intense optical beams under appropriate conditions.

4. CONCLUSION

In summary, we have demonstrated self-focusing of light in colloidal suspensions of gold nanorods over a wide range of pump wavelengths and in different solvent environments. We find a much smaller power is needed for the formation of solitons at the longitudinal surface plasmon resonance of the rods, and the soliton formation power in toluene suspensions is also significantly less than that in aqueous suspensions. Our results suggest that the optical scattering and absorption forces play a major role in soliton formation. By analyzing the optical forces and torque acting on the gold nanorods, we show theoretically that it is possible to align the nanorods inside a soliton channel with wavelength-dependent orientations. A theoretical estimate for the resulting synthetic optical anisotropy inside the soliton channel is also provided, although the expected synthetic anisotropic properties are too subtle to be observed through polarization transmission measurements of a low-intensity 1064 nm probe beam guided along the soliton channel. The ability to achieve tunable soliton formation and control nanorod orientations in colloidal nanosuspensions with low-power CW laser beams can be used to produce polarization-dependent transmission, which may lead to interesting applications in all-optical switching and transparent display technologies.

Funding. Army Research Office (ARO) (W911NF-15-1-0413); National Science Foundation (NSF) (PHY-1404510); National Key R&D Program of China (2017YFA0303800); National Natural Science Foundation of China (NSFC) (11504184).

REFERENCES

1. M. Kauranen and A. V. Zayats, "Nonlinear plasmonics," Nat. Photonics **6**, 737–748 (2012).
2. J. Butet, P.-F. Brevet, and O. J. F. Martin, "Optical second harmonic generation in plasmonic nanostructures: from fundamental principles to advanced applications," ACS Nano **9**, 10545–10562 (2015).
3. A. S. Reyna and C. B. de Araújo, "High-order optical nonlinearities in plasmonic nanocomposites—a review," Adv. Opt. Photon. **9**, 720–774 (2017).
4. N. C. Panoiu, W. E. I. Sha, D. Y. Lei, and G.-C. Li, "Nonlinear optics in plasmonic nanostructures," J. Opt. **20**, 083001 (2018).
5. N. M. Litchinitser, "Nonlinear optics in metamaterials," Adv. Phys. X **3**, 1367628 (2018).
6. G. A. Wurtz, R. Pollard, W. Hendren, G. P. Wiederrecht, D. J. Gosztola, V. A. Podolskiy, and A. V. Zayats, "Designed ultrafast optical nonlinearity in a plasmonic nanorod metamaterial enhanced by nonlocality," Nat. Nanotechnol. **6**, 107–111 (2011).
7. M. Mesch, B. Metzger, M. Hentschel, and H. Giessen, "Nonlinear plasmonic sensing," Nano Lett. **16**, 3155–3159 (2016).
8. Y. Hua, K. Chandra, D. H. M. Dam, G. P. Wiederrecht, and T. W. Odom, "Shape-dependent nonlinear optical properties of anisotropic gold nanoparticles," J. Phys. Chem. Lett. **6**, 4904–4908 (2015).
9. M. Gordel, J. Olesiak-Banska, R. Kolkowski, K. Matczyszyn, M. Buckle, and M. Samoc, "Shell-thickness-dependent nonlinear optical properties of colloidal gold nanoshells," J. Mater. Chem. C **2**, 7239–7246 (2014).
10. S. Fardad, A. Salandrino, M. Heinrich, P. Zhang, Z. Chen, and D. N. Christodoulides, "Plasmonic resonant solitons in metallic nanosuspensions," Nano Lett. **14**, 2498–2504 (2014).
11. T. S. Kelly, Y.-X. Ren, A. Samadi, A. Bezryadina, D. N. Christodoulides, and Z. Chen, "Guiding and nonlinear coupling of light in plasmonic nanosuspensions," Opt. Lett. **41**, 3817–3820 (2016).

12. A. S. Reyna and C. B. de Araújo, "Guiding and confinement of light induced by optical vortex solitons in a cubic-quintic medium," Opt. Lett. **41**, 191–194 (2016).
13. J. Trojek, L. Chvátal, and P. Zemánek, "Optical alignment and confinement of an ellipsoidal nanorod in optical tweezers: a theoretical study," J. Opt. Soc. Am. A **29**, 1224–1236 (2012).
14. J.-W. Liaw, W.-J. Lo, and M.-K. Kuo, "Wavelength-dependent longitudinal polarizability of gold nanorod on optical torques," Opt. Express **22**, 10858–10867 (2014).
15. K. C. Chu, C. Y. Chao, Y. F. Chen, Y. C. Wu, and C. C. Chen, "Electrically controlled surface plasmon resonance frequency of gold nanorods," Appl. Phys. Lett. **89**, 103107 (2006).
16. W. Ahmed, E. S. Kooij, A. van Silfhout, and B. Poelsema, "Quantitative analysis of gold nanorod alignment after electric field-assisted deposition," Nano Lett. **9**, 3786–3794 (2009).
17. P. Zijlstra, M. van Stee, N. Verhart, Z. Gu, and M. Orrit, "Rotational diffusion and alignment of short gold nanorods in an external electric field," Phys. Chem. Chem. Phys. **14**, 4584–4588 (2012).
18. J. Fontana, G. K. B. da Costa, J. M. Pereira, J. Naciri, B. R. Ratna, P. Palffy-Muhoray, and I. C. S. Carvalho, "Electric field induced orientational order of gold nanorods in dilute organic suspensions," Appl. Phys. Lett. **108**, 081904 (2016).
19. S. Etcheverry, L. F. Araujo, G. K. B. da Costa, J. M. B. Pereira, A. R. Camara, J. Naciri, B. R. Ratna, I. Hernández-Romano, C. J. S. de Matos, I. C. S. Carvalho, W. Margulis, and J. Fontana, "Microsecond switching of plasmonic nanorods in an all-fiber optofluidic component," Optica **4**, 864–870 (2017).
20. M. Maldonado, L. de Souza Menezes, L. F. Araujo, G. K. B. da Costa, I. C. S. Carvalho, J. Fontana, C. B. de Araújo, and A. S. L. Gomes, "Nonlinear refractive index of electric field aligned gold nanorods suspended in index matching oil measured with a Hartmann–Shack wavefront aberrometer," Opt. Express **26**, 20298–20305 (2018).
21. Q. Liu, Y. Cui, D. Gardner, X. Li, S. He, and I. I. Smalyukh, "Self-alignment of plasmonic gold nanorods in reconfigurable anisotropic fluids for tunable bulk metamaterial applications," Nano Lett. **10**, 1347–1353 (2010).
22. K. C. Ng, I. B. Udagedara, I. D. Rukhlenko, Y. Chen, Y. Tang, M. Premaratne, and W. Cheng, "Free-standing plasmonic-nanorod superlattice sheets," ACS Nano **6**, 925–934 (2012).
23. Q. Liu, Y. Yuan, and I. I. Smalyukh, "Electrically and optically tunable plasmonic guest-host liquid crystals with long-range ordered nanoparticles," Nano Lett. **14**, 4071–4077 (2014).
24. C. J. Murphy and C. J. Orendorff, "Alignment of gold nanorods in polymer composites and on polymer surfaces," Adv. Mater. **17**, 2173–2177 (2005).
25. J. Pérez-Juste, B. Rodriguez-Gonzalez, P. Mulvaney, and L. M. Liz-Marzan, "Optical control and patterning of gold-nanorod-poly(vinyl alcohol) nanocomposite films," Adv. Funct. Mater. **15**, 1065–1071 (2005).
26. J. Li, S. Liu, Y. Liu, F. Zhou, and Z.-Y. Li, "Anisotropic and enhanced absorptive nonlinearities in a macroscopic film induced by aligned gold nanorods," Appl. Phys. Lett. **96**, 263103 (2010).
27. K. E. Roskov, K. A. Kozek, W. C. Wu, R. K. Chhetri, A. L. Oldenburg, R. J. Spontak, and J. B. Tracy, "Long-range alignment of gold nanorods in electrospun polymer nano/microfibers," Langmuir **27**, 13965–13969 (2011).
28. H. Zhang, Z. Hu, Z. Ma, M. Gecevičius, G. Dong, S. Zhou, and J. Qiu, "Anisotropically enhanced nonlinear optical properties of ensembles of gold nanorods electrospun in polymer nanofiber film," ACS Appl. Mater. Interfaces **8**, 2048–2053 (2016).
29. M. Pelton, M. Liu, H. Y. Kim, G. Smith, P. Guyot-Sionnest, and N. F. Scherer, "Optical trapping and alignment of single gold nanorods by using plasmon resonances," Opt. Lett. **31**, 2075–2077 (2006).
30. C. Selhuber-Unkel, I. Zins, O. Schubert, C. Sönnichsen, and L. B. Oddershede, "Quantitative optical trapping of single gold nanorods," Nano Lett. **8**, 2998–3003 (2008).
31. L. Tong, V. D. Miljković, and M. Käll, "Alignment, rotation, and spinning of single plasmonic nanoparticles and nanowires using polarization dependent optical forces," Nano Lett. **10**, 268–273 (2010).
32. P. V. Ruijgrok, N. R. Verhart, P. Zijlstra, A. L. Tchebotareva, and M. Orrit, "Brownian fluctuations and heating of an optically aligned gold nanorod," Phys. Rev. Lett. **107**, 037401 (2011).
33. J. Do, M. Fedoruk, F. Jäckel, and J. Feldmann, "Two-color laser printing of individual gold nanorods," Nano Lett. **13**, 4164–4168 (2013).
34. Z. Li, W. Mao, M. S. Devadas, and G. V. Hartland, "Absorption spectroscopy of single optically trapped gold nanorods," Nano Lett. **15**, 7731–7735 (2015).
35. Y.-X. Ren, T. S. Kelly, C. Zhang, H. Xu, and Z. Chen, "Soliton-mediated orientational ordering of gold nanorods and birefringence in plasmonic suspensions," Opt. Lett. **42**, 627–630 (2017).
36. R. Karimzadeh, "Spatial self-phase modulation of a laser beam propagating through liquids with self-induced natural convection flow," J. Opt. **14**, 095701 (2012).
37. R. El-Ganainy, D. N. Christodoulides, C. Rotschild, and M. Segev, "Soliton dynamics and self-induced transparency in nonlinear nanosuspensions," Opt. Express **15**, 10207–10218 (2007).
38. R. El-Ganainy, D. N. Christodoulides, E. M. Wright, W. M. Lee, and K. Dholakia, "Nonlinear optical dynamics in nonideal gases of interacting colloidal nanoparticles," Phys. Rev. A **80**, 053805 (2009).
39. W. Man, S. Fardad, Z. Zhang, J. Prakash, M. Lau, P. Zhang, M. Heinrich, D. N. Christodoulides, and Z. Chen, "Optical nonlinearities and enhanced light transmission in soft-matter systems with tunable polarizabilities," Phys. Rev. Lett. **111**, 218302 (2013).
40. L. Novotny and B. Hecht, "Forces in confined fields," in *Principles of Nano-Optics* (Cambridge University, 2006), Chap. 13, pp. 427–428.
41. Q. Zhan, "Trapping metallic Rayleigh particles with radial polarization," Opt. Express **12**, 3377–3382 (2004).
42. P. M. Hansen, V. K. Bhatia, N. Harrit, and L. Oddershede, "Expanding the optical trapping range of gold nanoparticles," Nano Lett. **5**, 1937–1942 (2005).
43. F. J. V. Santos, C. A. Nieto de Castro, J. H. Dymond, N. K. Dalaouti, M. J. Assael, and A. Nagashima, "Standard reference data for the viscosity of toluene," J. Phys. Chem. Ref. Data **35**, 1–8 (2006).
44. J. W. P. Schmelzer, E. D. Zanotto, and V. M. Fokin, "Pressure dependence of viscosity," J. Chem. Phys. **122**, 074511 (2005).